Deep-Sea Research Part II 168 (2019) 104614

Contents lists available at ScienceDirect

Deep-Sea Research Part II

journal homepage: www.elsevier.com/locate/dsr2

Turbulence at the periphery of Sri Lanka dome

I. Lozovatsky[a,*], A. Pirro[a], E. Jarosz[c], H.W. Wijesekera[c], S.U.P. Jinadasa[d,e], H.J.S. Fernando[a,b]

[a] Department of Civil & Environmental Engineering and Earth Sciences, University of Notre Dame, USA
[b] Department of Aerospace and Mechanical Engineering, University of Notre Dame, USA
[c] Naval Research Laboratory, Stennis Space Center, USA
[d] Ocean University, Mattakuliya, Colombo, Sri Lanka
[e] National Aquatic Resources Research and Development Agency, Colombo, Sri Lanka

A B S T R A C T

Measurements of kinetic energy dissipation rate ε and other oceanographic variables (temperature, salinity, density, and current profiles) were conducted at 20 stations along a 90 nautical mile section at the southwestern periphery of Sri Lanka Dome (SLD), which is a mesoscale cyclonic eddy that usually appears in Bay of Bengal to the east of Sri Lanka during summer monsoons. The broad aim was to document and interpret the structure of flow and turbulence in SLD and quantify turbulent mixing therein using parametric studies. A tendency of upward doming (upwelling) of the pycnocline toward the SLD center is observed, leading to substantial shallowing of the mixed layer therein, with the mixed layer depth decreasing from ~40 m outside the SLD to ~10–15 m inside the cyclonic eddy. The cumulative distribution of ε in the SLD pycnocline (below 40 m depth) is well approximated by the Burr probability distribution. A high level of ε in the pycnocline was observed at the inner periphery of SLD, concurrent with low values of gradient Richardson numberRi. A parameterization for eddy diffusivity in the SLD pycnocline as a function of Ri is suggested.

1. Introduction

Quantification of mixing in the northern Indian Ocean, especially in the Bay of Bengal (BoB), is crucial for understanding and predicting vertical exchanges of heat, mass, momentum, and biogeochemical fluxes between the deep ocean and surface waters (Wijesekera et al., 2016a). The thermohaline structure of BoB is complex, and often there is a disparity between the temperature-based and the density-based mixed layer depths. The former is deeper, allowing heat to be stored in the so-called barrier layer between the two. This layer usually occupies a narrow depth range (between ~ 15 and 30 m), originating mainly due to the enormous volume of the river runoff (i.e. Brahmaputra, Irrawaddy, Ganges and Godavari rivers) and heavy monsoon precipitation. River runoff is strongest in the summer, spreading widely over the northern part of the Bay while mixing with ambient ocean water both vertically and horizontally (Akhil et al., 2014). The barrier layer is wide spread in the northern and central BoB and Sri Lanka coastal waters (Girishkumar et al., 2011) but it is less frequent in the southern BoB during the summer monsoon, where the depths of surface isothermal and isohaline layers coincide with the mixed layer depth (e.g. Lozovatsky et al., 2016).

The two main seasonal features of large-scale circulation in the BoB are the East India Coastal Current (IECC) directed southward during northeastern monsoon and the Southwest Monsoon Current (SMC) directed past the southern coast of Sri Lanka to BoB during southwest monsoon (Shetye, 1993; de Vos et al., 2014; Wijesekera et al., 2015).

The convergence and divergence of currents as well, as their *reversals* during the monsoon transition result in the development of a variety of mesoscale features such as filaments, meanders and eddies (Shetye et al., 1996; Shroyer et al., 2016). Some well recognizable mesoscale features of BoB are a large cyclonic eddy to the east of Sri Lanka known as the Sri Lanka Dome (SLD; Fig. 1) with a negative sea surface height anomaly (SSHA) and an anticyclonic eddy (AE) to the southeast of it with positive SSHA. It has been suggested that SLD develops in response to upwelling of pycnocline under a cyclonic wind stress curl (e.g. Vinayachandran and Yamagata, 1998; Das et al., 2016; Jensen et al., 2018). Analysis of SSHA retrieved from AVISO satellite-image archive and drifter trajectories suggest that SLD originates toward the end of May, fully develops in the second part of June, and starts spreading and moving slightly northwest with approximate speed of 3 nautical miles per day in early July (2014 observations, Lozovatsky et al. (2016)). The presence of more saline and slightly cooler waters in the surface layer is linked to the circulation associated with the SLD. Fig. 1 shows a SSHA view of SLD in mid-July 2018, where an elongation of SLD can be seen along the northeastern-southwestern axis. Both vertical and horizontal mixing affect salinity and temperature structure of the surface mixed layer (ML), the mixed layer depth (MLD) and fluxes between the ocean interior and ML. Although Jinadasa et al. (2016) have analyzed specific features of turbulence in relation to frontal dynamics in the northern BoB and across EICC and SMC, no

* Corresponding author. Department of Civil and Environmental Engineering and Earth Sciences, University of Notre Dame, Notre Dame, IN, 46556, USA.
E-mail address: i.lozovatsky@nd.edu (I. Lozovatsky).

https://doi.org/10.1016/j.dsr2.2019.07.002
Received 30 January 2019; Received in revised form 6 July 2019; Accepted 7 July 2019
Available online 11 July 2019
0967-0645/

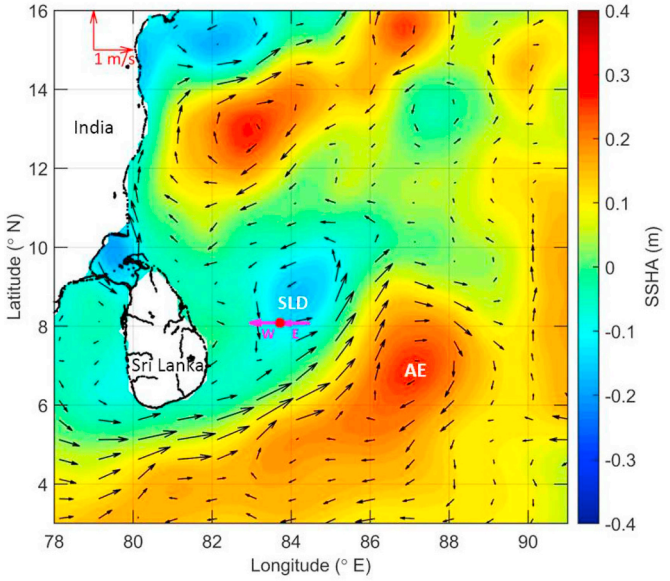

Fig. 1. Contour plot of the sea surface height anomaly in the southern BoB on July 15, 2018. Twenty VMP stations were taken along two sections (10 stations per section, 5 nautical miles apart) in the direction shown by magenta arrows away from (sub-section W - July 15–16) and toward (sub-section E – July 16–17) the long-term mooring (red dot). The approximate location of the Sri Lanka Dome is marked as SLD; AE is an anticyclonic eddy southeast of SLD. (For interpretation of the references to color in this figure legend, the reader is referred to the Web version of this article.)

measurements of small-scale turbulence in SLD area have been reported yet.

The sea surface temperature (SST) in southern BoB is substantially affected by mesoscale features such as SLD (Vinyachandran and Yamagata, 1998) and AE, and hence mesoscale dynamics ought to be a major element determining the oceanic control of atmospheric convection in BoB. Boreal Summer Intraseasonal Oscillations (BSISO) and Monsoon Intraseasonal Oscillations (MISO) in BoB, therefore, are expected to be influenced by the SLD and AE (Bhat et al., 2004; Girishkumar et al., 2017). As such, during a special 2018 oceanic field campaign designed to study MISO events, dubbed MISO-BOB, we collected data on the turbulent kinetic energy (TKE) dissipation rate ε and other oceanographic variables (stratification, currents) in the proximity of SLD to study vertical mixing and transport processes. Since the field expedition was primarily dedicated to deploy five deep ocean moorings, only limited time was available for profiling, and only the dome's periphery could be covered within logistical constraints. The results reported herein provide first insight into directly-evaluated ε in the SLD area, which helps gain a better understanding of small-scale physical processes in the southern BoB by estimating such mixing parameters as the eddy diffusivity $K_N \sim \gamma\varepsilon/N^2$ and the relationship between K_N and gradient Richardson number . Such parameterizations are paramount for ocean modeling, as they sensitively determine predicted large-scale circulation (e.g., Pacanowski and Philander, 1981; Cummins et al., 1990). Here $N^2 = (g/\rho_0) \times (d\rho_\theta/dz)$ and $Sh^2 = (d\overline{u}/dz)^2 + (d\overline{v}/dz)^2$ are the squared buoyancy frequency and squared mean vertical shear, respectively, $\overline{u}$ and $\overline{v}$ the zonal and meridional components of the mean flow, γ a mixing efficiency (see Lozovatsky and Fernando, 2013), and g, ρ_θ, ρ_0 are the gravitational acceleration, potential and reference densities, respectively; z is positive downwards.

Because spatial (and temporal) intermittency is an intrinsic quantity of ocean turbulence related to a stochastic nature of turbulence generation at different depths, the cumulative distribution functions of ε in the SLD pycnocline is also analyzed in this paper.

2. Measurements

The measurements were conducted on board the R/V Thomas G. Thompson as a part of the 2018 MISO-BOB field campaign sponsored by the Office of Naval Research and the Naval Research Laboratory. The campaign consisted of two cruise legs, and the measurements reported here were part of the second leg (June 28 – July 21) dedicated to deploy five deep moorings to observe oceanic intraseasonal oscillations (ISO) over a year. Eight surface drifters were deployed inside the SLD (8°5′N, 83°43′E), and a towed underway-survey was conducted using a ScanFish. Twenty four deep CTD profiles were collected along the ship track, some coinciding with microstructure measurements, along with water sampling and plankton net sampling.

The microstructure survey was conducted in the vicinity of SLD. A Vertical Microstructure Profiler (VMP-500; http://rocklandscientific.com/products/profilers/vmp-500/) was used for measurements, which were taken along 8°4′N (the W-E transect), in the depth range from the surface to a depth ~ 125–165 m. The VMP is a tethered, nearly free-falling instrument, which measures high-frequency, small-scale components of velocity shear du'/dz and dv'/dz to quantify ocean turbulence. It carries two airfoil probes (to estimate ε), a two-axis accelerometer, pressure sensor (depth) and a Seabird temperature-conductivity unit to obtain precise estimates of temperature, salinity, and potential density. The data processing followed the methodology described in Roget et al. (2006). Microstructure data above 8 m were discarded due to possible ship-wake contamination.

A 90 nautical mile long latitudinal transect with 20 VMP stations, each 5 miles apart, was carried out along 8°4′N from 83°43′E to 82°58′E (western section), which started at 14:50 on July 15 and ended at 2:00 on July 16, 2018, and from 84°29′E to 83°43′E (eastern section) that started at 19:15 on July 16 and ended at 4:30 on July 17, 2018 UTC. The two sections (10 stations each) were taken to the west and to the east from a long-term mooring shown by a red dot in Fig. 1. According to the SSHA map, which indicates only the approximate position of SLD, the VMP measurements were taken at the southwestern periphery of SLD (Fig. 1); both sections W and E were directed westward. Note that the satellite AVISO data of SSHA and corresponding geostrophic velocities (https://www.aviso.altimetry.fr/en/data/products.html) are of relatively low spatial (0.25°) and temporal (1 day) resolution, and based on specific data averaging of past images taken during past several days).

The shipboard standard meteorological measurements, including uptake of the underway sea surface temperature and salinity (at ~3 m depth), and 150 kHz ADCP (Acoustic Doppler Current Profiler) data were collected along the VMP transect. The variations of ADCP zonal $u(z, t)$ and meridional $v(z, t)$ velocity components during sailing along the western and eastern sections are shown in Fig. 2, where the positions (times) of VMP stations are specified in the upper panels of the plot. The ADCP currents show a south/southeast directed flow along most of the western section, specifically in the upper ~60 m layer, which can be further traced up to the middle of the eastern section. From this point, the northern current component starts to dominate, first below z ~90 m, but then positive $v(z, t)$ occupies the entire water column depicting a northeast directed flow closer to eastern end of the eastern section. The flow patterns support the notion that VMP measurements were taken at the southern periphery of SLD. The ADCP currents are in general agreement with surface geostrophic currents (Fig. 1) retrieved from the SSHA data (the south/southeast directed current vectors cross the western VMP section, while the north-east directed vectors cross the eastern section shown in Fig. 1).

The TKE dissipation rate $\varepsilon(z)$ profiles were estimated using ~1.4 m vertical spacing (2 s time averaging, ~0.7 ms^{-1} sinking velocity). The same spacing was adopted for temperature $T(z)$, salinity $S(z)$ and specific potential density $\sigma_\theta(z)$ profiles; the squared buoyancy frequency $N^2(z)$ was calculated by depth-sorted profiles of $\sigma_\theta(z)$. To obtain profiles of squared shear $Sh^2(z)$, a 8 m, 5 min ADCP grid of $u(z, t)$ and

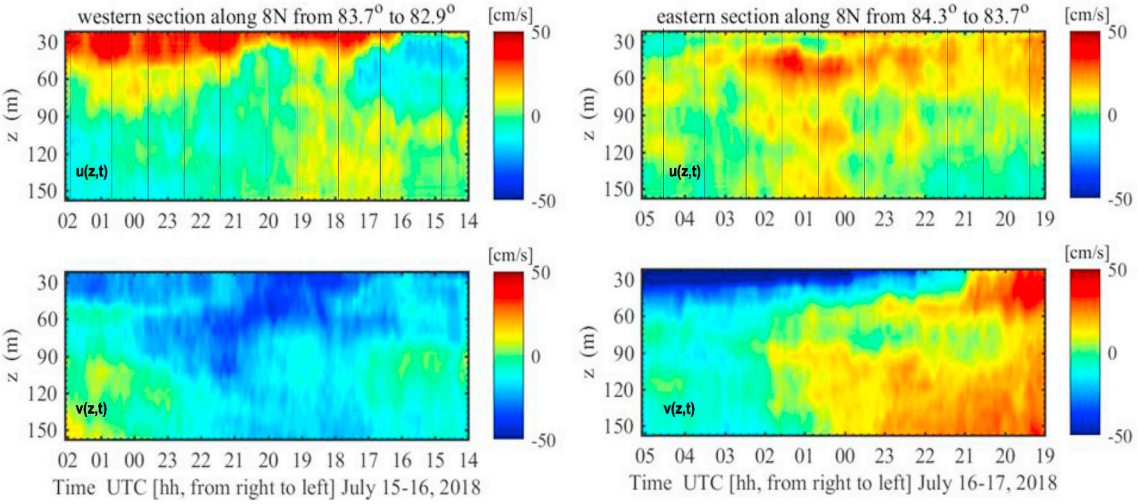

Fig. 2. ADCP velocity components $u(z, t)$ (upper) and $v(z, t)$ (lower) panels along western (left) and eastern (right) sections of the VMP measurements. Times correspond to VMP casts are indicated in the upper panels by vertical lines.

$v(z, t)$ was setup with interpolation to the time and depths of VMP casts used to calculate $N^2(z)$ profiles. The local Richardson numbers and corresponding diffusivities K_N along the E-W transect were then calculated.

3. Results

3.1. Stratification and mixed layer depth

The salinity $S(z, x)$ in the upper 125 m of the water column is shown in Fig. 3 (lower panel) along the 90 n.m. (nautical miles) cross-section centered at the mooring location, $x = 0$. The colored salinity contour plot overlapped by contours (black lines) of specific potential density $\sigma_\theta(z, x)$ displays a sloping halocline uplifted generally from the west to the east. The halocline coincides with a sharp density interface (density jump) between the near surface ML and an underlying seasonal pycnocline. The squared buoyancy frequency in the pycnocline below the density jump is $N_o^2 \approx (1.5 - 2.3) \times 10^{-4} s^{-2}$. The thickness of the density jump (the layer where N^2_{max} approaches $10^{-2}\ s^{-2}$) varied along the transect, widening, on the average, from ~7 m at the most western station to ~ 12 m at the most eastern station. The elevation of the sharp halocline from depth z ~40–45 m at x = - 45 n.m. to z ~10–15 m at x = 45 n.m. is the most prominent feature of stratification along 8°4′N, pointing to the doming influence of cyclonic circulation associated with SLD. Fig. 3 suggests that 4 VMP stations at the western end of transect (between $x = -45$ and -30 n.m.) were sampled outside the SLD, while two most eastern stations (x = 40 and 45 n.m.) were closer to the SLD center. Note that the SSHA map in Fig. 1 indicates that the approximate position of SLD center is to the north of the VMP transect. SSHA maps are based on fairly low-resolution satellite data, and relatively coarse interpolation may have led to a mismatch between in situ measurements and satellite imagery.

The sea surface temperature (SST) and salinity (SSS) tracks in Fig. 3 (upper panel) are consistent with the notion that 6–7 eastern stations (x ~ 20–45 n.m.) are directly affected by SLD dynamics, leading to a continuously eastward decrease of SST from ~28.89 °C to ~28.37 °C over ~ 25 n.m. (toward expected center of SLD). Over the same time/distance, SSS increased from ~33.89 to ~34.15. At the outskirts of SLD (between x ~ 10 and -25 n.m.), the SST and SSS (to a lesser extent) remained relatively constant (~28.95 °C and ~33.97), but SSS starts to go up between x = - 25 and x = - (35–40) n.m. at the stations presumably influenced by a surface saline filament.

The mixed layer depth (MLD) along the transect was also substantially affected by SLD dynamics. Note that here the mixed layer was defined as the depth range between the sea surface and a particular depth z_D where variations of specific potential density do not exceed $\delta\sigma_\theta = 0.02$ (e.g., Peters et al., 1988; Padman and Dillon, 1991; Lozovatsky et al., 2005). A substantially larger MLD = (35–39) m observed at most western stations compared to MLD ~ 23 m at central stations (Fig. 3, middle panel) indicates that these most western stations were taken outside the SLD. Fig. 3 also shows that starting from x = (15–20) n.m. of the eastern section, the MLD continuously shallowed from ~20 m to 10 m towards the SLD owing to the doming pycnocline associated with cyclonic circulation of SLD.

Pollard et al. (1972) suggested that the depth of the mixed boundary layer induced in stratified ocean by a constant wind stress specified by friction velocity u_* (in our case calculated using the sea-mat/air-sea Matlab toolbox based on wind speed at 10 m above the sea surface) can be scaled as $z_{ML} = 1.7 L_{fN}$, where $L_{fN} = u_*/\sqrt{fN_o}$, f the Coriolis frequency and N_o a characteristic buoyancy frequency in the pycnocline. It appears that the measured MLD z_D and the length scale z_{ML} are comparable only at several central stations (Fig. 3, middle panel), and they substantially diverge from each other closer to the western and eastern edges of the transect but in the opposite directions. Much shallower z_D compare to z_{ML} is observed at x = (30–45) n.m. with highest difference being ~ 20 m. This strongly suggests that close to the SLD core the mixed layer was shallowed by SLD doming. Therefore, the wind stress curl and planetary wave dynamics responsible for SLD cause a simple mixed layer formulation to be invalid. On the contrary, to the west (between $x = -45$ n.m. and $x = -25$ n.m.), the observed MLD was 14–18 m deeper than calculated z_{ML} = (20–21) m. This indicates that local wind (W_a = 10 ms^{-1} maximum, see Fig. 4) was unable to produce this deep ML with z_D = (35–39) m. The surface boundary layer therein was probably advected to the measurement site from a region previously affected by higher winds. Note that MLD in Bay of Bengal is highly variable in time and space not only due to variation of atmospheric forcing but also due to regional mesoscale dynamics. In the northern part of the Bay, the surface mixed layer is relatively shallow (MLD = 10–30 m), being strongly affected by large inflow of fresh riverine water (Parampil et al., 2010). Much deeper MLD = (80–90) m was observed in the southern BoB (Wijesekera et al., 2016b), and this region is affected by a large anticyclonic eddy that downwells the pycnocline. For typical summer monsoon winds of (10–12) ms^{-1}, the wind-induced MLD at 8°4′N is about (20–25) m, as was observed during the current study (July 2018), as well as during a July 2014 cruise (Lozovatsky et al., 2016) that conducted measurements 100 n.m. to the east from the current location. It was also shown that short internal waves with characteristic height 3–5 m affect MLD in the southern BoB,

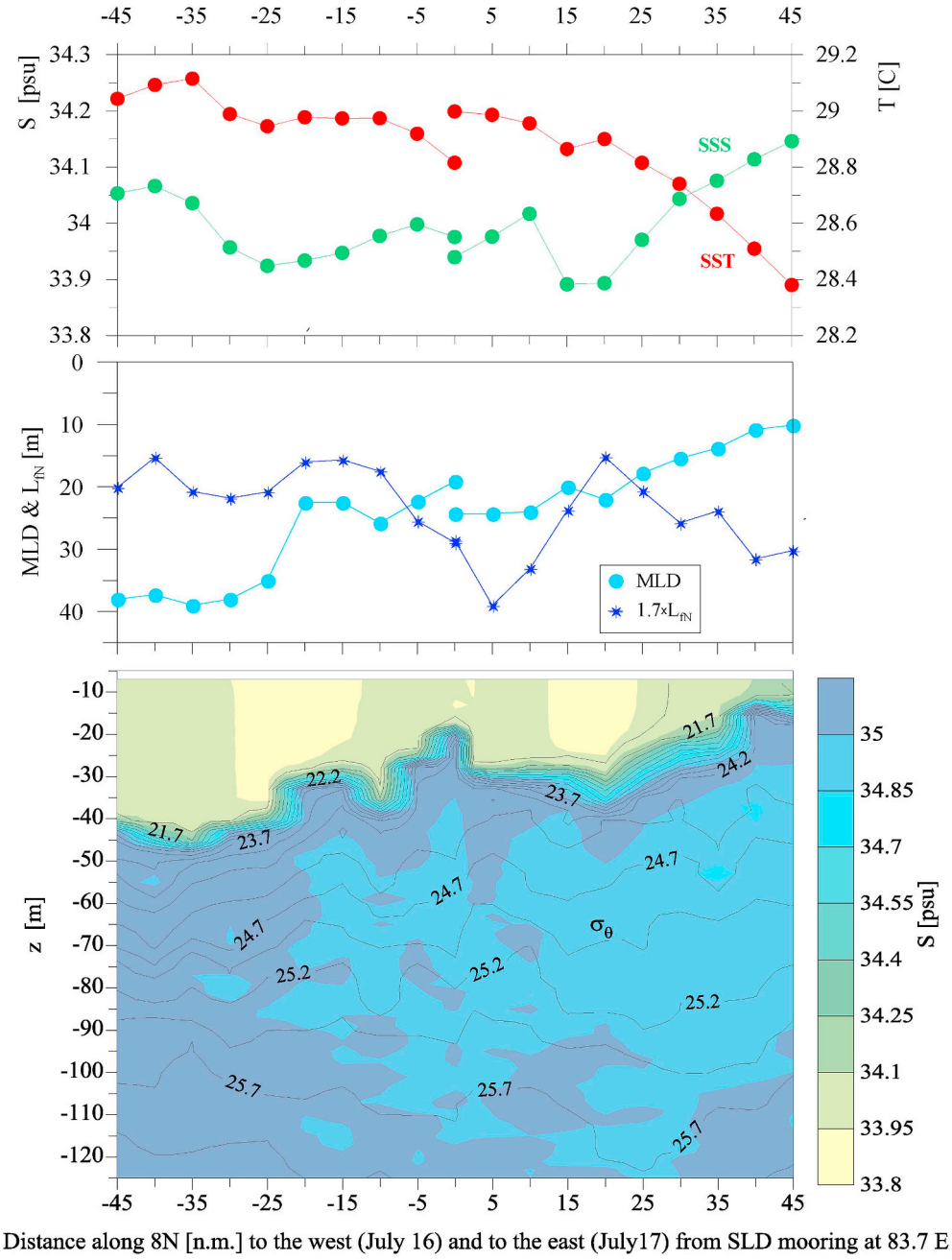

Fig. 3. Salinity contour plot (colors) overlaid by contours of specific potential density σθ (lower panel); the mixed layer depth (MLD) and a characteristic (Pollard et al., 1972) mixed layer scale $1.7 \times L_{fN}$ (middle panel), and the sea surface temperature SST and salinity SSS (upper panel) along 8°4′N between 82°58′E and 84°29′E. (For interpretation of the references to color in this figure legend, the reader is referred to the Web version of this article.)

which could cause the observed mismatch between MLD at the first station of the western station, $z_D = 19$ m, and the last station of the eastern station, $z_D = 24$ m, at $x = 0$.

3.2. TKE dissipation rate

3.2.1. Mixed layer turbulence

Profiles of the TKE dissipation rate $\varepsilon(z)$ at VMP stations (color bars) are given in Fig. 4 (lower panels), separately for the west (July 15–16) and east (July 16–17) sections shown in Fig. 1. During the measurements, the wind speed W_a on the average varied from 4.5 (min) to 12.5 (max) ms^{-1} (Fig. 4, upper panels).

Consistent with previous turbulent measurements in BoB (Jinadasa et al., 2016), the near-surface layer (where ε mostly exceeded 10^{-7} Wkg^{-1}) was found to be effectively decoupled from the water interior by a narrow sharp density jump, which is depicted in Fig. 4 by contours of specific potential density $\sigma_\theta(z)$ that overlay the dissipation profiles. On July 16–17, the ML turbulence (east section) was generated and sustained by wind speeds W_a exceeding ~ 8 ms^{-1}. Toward the end of the eastern section (closer to the mooring), the deepening of ML and increase of ML turbulence in space/time (x = 5–10 n.m.) correlated with the increase of W_a up to ~ 12 ms^{-1}. On the other hand, the dissipation in ML did not decline much and did not respond quickly enough to a relatively short (less than 2 h) drop of W_a to ~ 5 ms^{-1} (Fig, 4, x between ~ 25 and 15 n.m.). A similar situation was observed on July 15–16 at the first half of the western section ($0 > x > -20$ n.m.) when W_a decreased from ~9 to 5 ms^{-1}, wherein turbulence in a quite shallow ML (< ~20 m) did not respond quickly. When the mixed layer depth

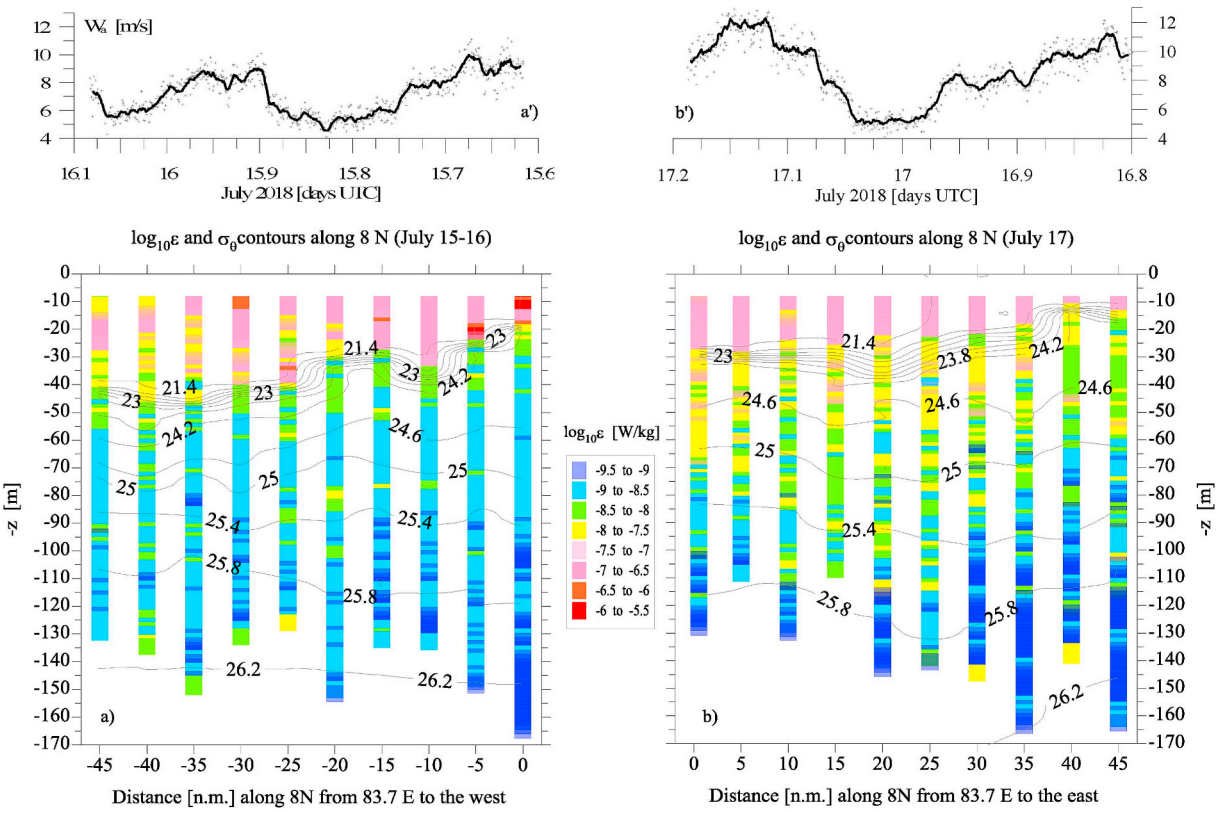

Fig. 4. TKE dissipation rate (color bands) and density contours along 8°4′N 45 n.m. to the west (a) and to the east (b) of the SLD mooring at 83.7°E. Upper panels: the shipboard wind speed (15 m above the sea surface) along the western (a') and eastern (b') VMP sections (symbols - 1 min averaged data, adjusted to 10 m above sea surface; heavy lines - 10 min running averages). (For interpretation of the references to color in this figure legend, the reader is referred to the Web version of this article.)

showed a sharp increase from about 20 m to (35–40) m over the 5 most western stations, however, the dissipation rate in the ML became more intermittent, generally responding to local variations of the wind stress. Patches of lower turbulence levels appeared in the deep ML during wind weakening from 9 to 5 ms^{-1} at $x = -25$ and -40 n.m., suggesting, as expected, that the redistribution of turbulence in a deeper ML is more intermittent than in a shallow ML.

3.2.2. *Turbulence in the pycnocline*

The dissipation rate profiles in Fig. 4 indicate that stratified ocean interior below the density interface ($z > 40$ m) is less turbulent along the western section compared to the eastern section, which is shown in Fig. 4 by a larger numbers of yellow and light green layers in the right panel, specifically just below a narrow density jump displayed in Fig. 4 between 21.4 and 24.2 density contours. The statistical difference between dissipation rates in the stratified interior ($z > 40$ m) along western and eastern sections can be specified by cumulative distribution functions $CDF(\varepsilon)$ shown in Fig. 5. Both empirical $CDF(\varepsilon)$ are well approximated by the Burr probability distribution advocated by Lozovatsky et al. (2017) for turbulence in ocean pycnocline. The Burr (type XII) cumulative distribution function $CDF(\varepsilon)$ is

$$CDF_B(\varepsilon) = 1 - (1 + (\varepsilon/\varepsilon_0)^c)^{-k}, \quad (1)$$

where both $c > 0$ and $k > 0$ are shape parameters and $\varepsilon_0 \equiv \alpha_B$ is a scale parameter; $\varepsilon > 0$ by definition. The empirical probability of low ε (below the median value) is the same for both populations, but the probability of higher ε (above the median) is larger for the eastern section (see Fig. 5 for details). By analyzing $CDF(\varepsilon)$ in the pycnocline of the East China Sea, Gulf Stream, and the northern BoB, Lozovatsky et al. (2017) pointed out a possible inverse relationship between shape parameters of $CDF_B(\varepsilon)$, namely $c = A_0/k$, where A_0=1.26 is a regression

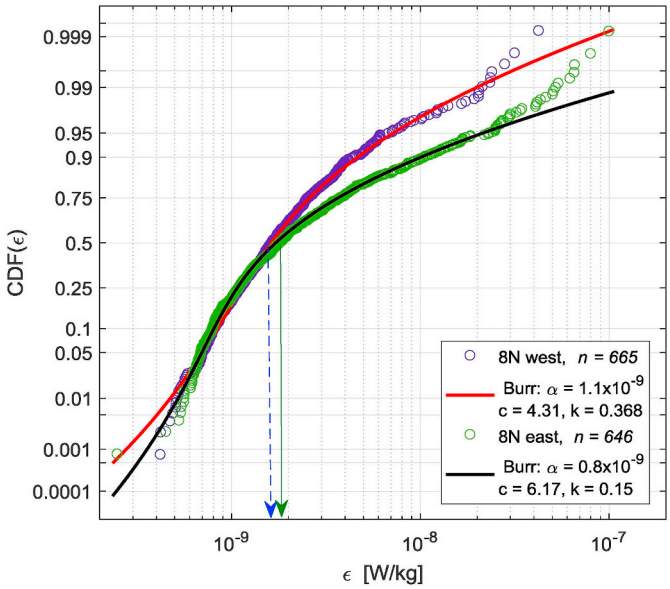

Fig. 5. Cumulative distribution functions of the dissipation rate in the pycnocline ($40 < z < 170$ m) along the western (blue circles) and eastern (green circles) VMP sections (see Figs. 1, 2 and 4). Parameters of corresponding approximations by the Burr model (red and black lines) are in the legend, n the number of samples. The corresponding median values $med(\varepsilon_{west}) = 1.64 \times 10^{-9}$ Wkg^{-1} (blue dashed arrow) and $med(\varepsilon_{east}) = 1.81 \times 10^{-9}$ Wkg^{-1} (green arrow). Note the lognormal scale along the vertical axis. (For interpretation of the references to color in this figure legend, the reader is referred to the Web version of this article.)

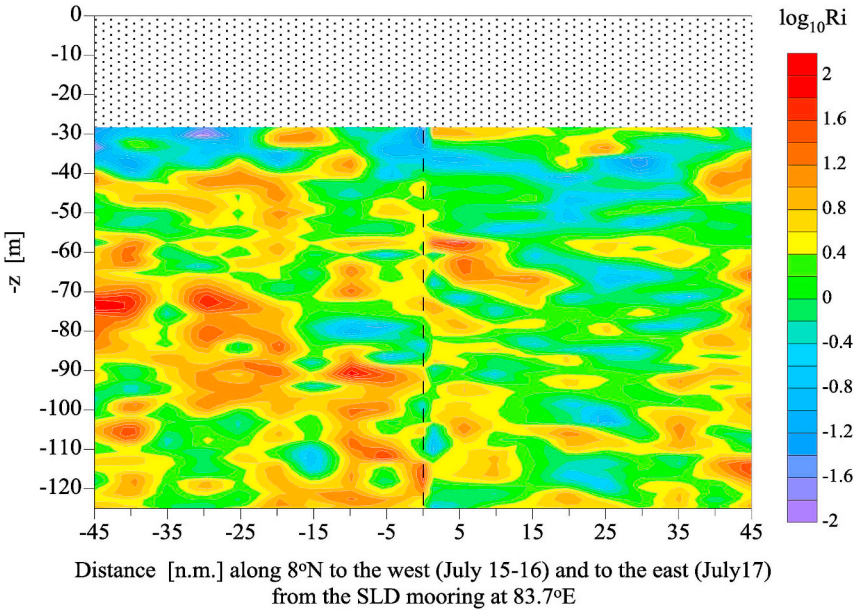

Fig. 6. Contour plot of the logarithm of gradient Richardson number $\log_{10}Ri$ along eastern (right of the black dashed line) and western VMP transects (no ADCP data in the blanked area).

coefficient with 95% confidence bounds (1.05, 1.57). The shape parameters of the distributions shown in Fig. 5 give the corresponding ratio $c \approx A/k$ with $A_W = c_W k_W = 1.58$ (western) and $A_E = c_E k_E = 0.93$ (eastern) sections. While A_W almost coincides with the upper limit of A_0 variability, the estimate of A_E deviates by about 10% from the lower limit of A_0 95% confidence bounds. This suggests that SLD dynamics modifies shape parameters of the dissipation rate probability distribution by an extent that exceeds statistical uncertainties.

Higher turbulence levels in the stratified interior at most stations of the eastern section generally correlates with lower gradient Richardson numbers for $x > 0$ compared to $x < 0$ (Fig. 6). Indeed, the median Ri in the depth range (30–125) m calculated using the full subset of data along the eastern section ($x > 0$) $med(Ri_{east}) = 1.87$ is about 60% of the $med(Ri_{west}) = 3.13$ for the western section ($x < 0$). Note the larger values of $Ri(z)$ at $x = 40$–45 n.m. observed inside SLD (yellow-orange area across the pycnocline), but much smaller $Ri(z)$ values are found in the middle of the eastern section (predominantly green-blue area between $x = 35$ and 15 n.m.). This segment could be associated with the internal periphery of SLD, where sheared currents are supposed to be stronger compared to SLD core (also see Fig. 2 that indicates a higher horizontal shear at the inner periphery of SLD). This notion requires further observations and analysis based on multiple sections across the entire SLD.

From the probabilistic point of view, the generation/dissipation of energetic turbulence in the stratified interior of SLD, which is effectively detached from the sea surface, can be considered as a random sequence of rare turbulent events. The sources of such turbulence is probably associated with non-stationry, intermittent internal-wave breaking and sporadic shear-induced instabilities (Jinadasa et al., 2016). Intensification of both vertical and horizontal shears generated by cyclonic mesoscale eddies like SLD could elevate turbulence and mixing compared to areas of low mesoscale activity.

3.2.3. Eddy diffusivity vs. the Richardson number

As discussed above, and has been reported by Lozovatsky et al. (2016), the shear-induced turbulence in the BoB seasonal pycnocline related to summer monsoon dynamics is an important source of diapycnal mixing in the southern BoB. As such, it is instructive to investigate the relationship between turbulent eddy diffusivity K_N and the gradient Richardson number, as has been done in numerous publications (e.g. Munk and Anderson, 1948; Pacanowski and Philander, 1981; Peters et al., 1988; Soloviev et al., 2001; Lozovatsky et al., 2006; Lozovatsky and Fernando. 2013). The bin-averaged estimates of $K_N = 0.2\varepsilon/N^2$ calculated for the entire data set (west and east sections together, Fig. 7) are shown in Fig. 8 as a function of the bin-averaged Richardson number. The bin-averaging (30 original samples per bin from presorted samples of the Richardson numbers Ri_s and corresponding samples ofK_N) was introduced to obtain a robust representation of $K_N(Ri)$. Although the scatter in Fig. 8 is still not small, a general trend of K_N reduction with increasing Ri is evident, with data reasonably following the formula

$$K_N = \frac{K_o}{(1 + Ri/Ri_{cr})^s} + K_b \tag{2}$$

where turbulence in neutrally stratified flow is represented by $K_o = 1.19 \times 10^{-4}$ m^{2}s^{-1} and for background conditions by $K_b = 10^{-6}$ m^{2}s^{-1}, with $Ri_{cr} = 0.25$ denoting the critical Ri. The power $s = 2$ used for the fitting is adopted from Lozovatsky and Fernando (2013), although the authors analyzed mixing in stably-stratified atmospheric boundary layer. The accuracy of the approximation specified in Fig. 8 by 95% confident bounds of K_o, the coefficient of determination $r^2 = 0.9$, the squared errors of prediction SSE, and the standard deviation of the residuals RMSE suggest that the agreement between the data and formula (2) is reasonably good, which indicates robustness of (2) for mixing in stratified flows. Note that damping of mixing in SLD pycnocline is quantified here by $s = 2$, which is stronger than that reported by Pelegri and Csanady (1994) for the western Atlantic and Paka et al. (1999) for the western equatorial Pacific ($s = 3/2$). Ours ($s = 2$) is the same as that suggested in Lozovatsky et al. (2006) for stratified layer in North Atlantic, but it is slightly weaker than that offered by Peters et al. (1988), $s = 2.5$, for mixing in the eastern equatorial Pacific.

Following Lozovatsky et al. (2006) it is possible to show that $s = 2$ provides a reasonable asymptote for the eddy diffusivity in non-stratified shear flows (i.e., homogeneous boundary layers) as well as in fully stratified non-sheared flows (i.e., grid generated turbulence). Formula (2) can be rewritten as

$$K_N = \frac{K_o}{(1 + Ri/Ri_{cr})^{s-1}} \mathrm{Pr}_t^{-1} + K_b, \tag{2a}$$

where Pr_t is the turbulent Prandtl number, which is commonly

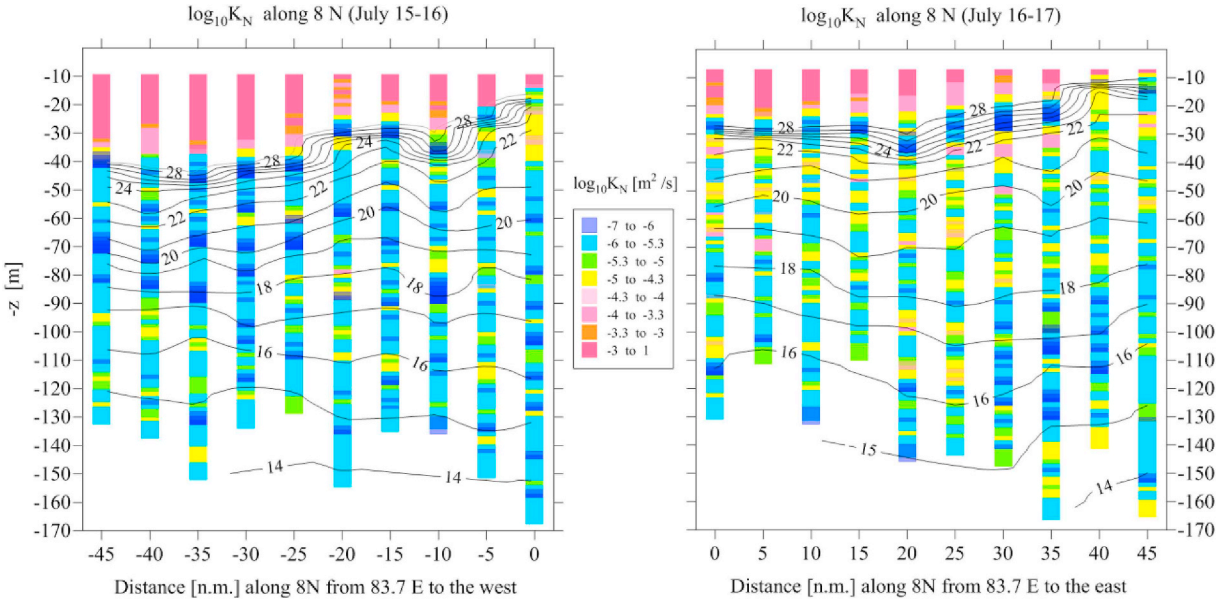

Fig. 7. The eddy diffusivity $K_N = 0.2\varepsilon/N^2$ profiles (color bands) and temperature contours along 8°4′N 45 n.m to the west (left panel) and to the east (right panel) of the SLD mooring at 83.7°E. High K_N values above the thermocline are in circumspect due to very small values of N^2in the surface mixed layer. (For interpretation of the references to color in this figure legend, the reader is referred to the Web version of this article.)

expressed in the following functional form of *Ri*:

$$\mathrm{Pr}_t^{-1} \equiv K_N/K_M \sim 1/(1 + Ri/Ri_c), \tag{3}$$

where K_N and K_M are the eddy diffusivity and viscosity, respectively, and Ri_c and Ri_{cr} are certain critical Richardson numbers, which may not have the same numerical values; for simplicity, however, we assume that they are equal. Specifying the eddy viscosity in a non-stratified sheared flow by turbulent kinetic energy q^2 or the dissipation rate ε and vertical shear *Sh*, as $K_{Mo} \sim q^2/Sh$, or $K_{Mo} \sim \varepsilon/Sh^2$ (e.g., Peters et al., 1988) and using $s = 2$ in formula (2a), we arrive at the well accepted asymptotic formulas of eddy viscosity in the limit of ($Ri \gg Ri_{cr}$): or $K_M \sim \varepsilon/N^2$. The above asymptotic forms for K_M are in agreement with the assumption that in a stratified flow, the outer turbulence scale l_{tr} should be proportional to the buoyancy Ozmidov-Dougherty scale, $L_0 = \varepsilon^{1/2}/N^{3/2}$, thus yielding $K_M \sim l_{tr}\sqrt{q^2}$. These scaling arguments favor a damping power $s = 2$ in formula (2) compared to the other empirical values.

4. Summary

Measurements of turbulent kinetic energy (TKE) dissipation rate ε were carried out during summer monsoons at the southwestern

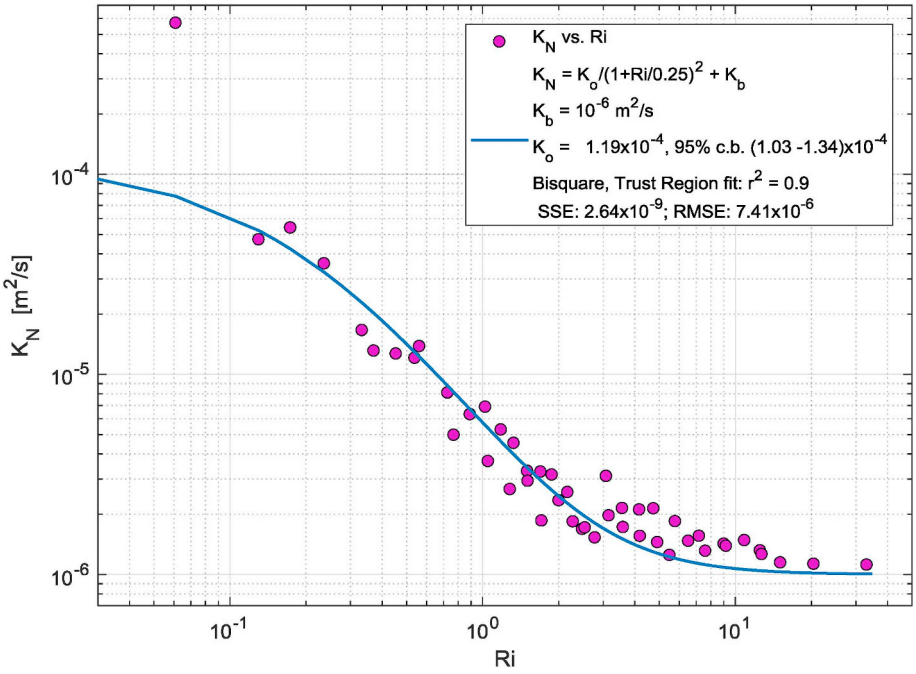

Fig. 8. Eddy diffusivity K_N as a function of the gradient Richardson number *Ri* approximated by formulae (2) using the Bisquare method and trust region algorithm (Matlab cftool, https://www.mathworks.com/help/stats/robustfit.html). Parameters of the fit (Eq. (2)) are in the legend along with the 95% confident bounds (c.b.) for K_o. The sum of squared errors of prediction (SSE) and the standard deviation of the residuals (RMSE - root mean square error) are also listed.

periphery of Sri Lanka Dome (SLD) located east of Sri Lanka in the southern Bay of Bengal. The measurement transect was along the latitude $\phi\varphi = 8^{\circ}4'$E, 90 nautical miles long in total, that consisted of two sections on either side (east and west) of the longitude $\lambda = 83^{\circ}4'$E, with each section having 10 VMP stations. The main findings are as follows:

1. Cyclonic circulation associated with Sri Lanka Dome (SLD) triggered an outcrop (upwelling) of a halocline at the SLD center with an average slope of about 30 m over 100 km (60 n.m.). Doming of the sharp density interface between surface mixed layer and stratified water interior (layer where $N^2_{\max}$ approaches 10^{-2} s^{-2}) led to substantial shallowing of the mixed layer depth from ~40 m outside the SLD to ~10–15 m closer to its core.
2. The TKE dissipation rate was found to be substantially higher at VMP stations that presumably occupy the inner periphery of SLD - that is about 10–25 n.m. away to the west from the expected SLD core. Relatively low values of gradient Richardson number Ri were also observed at the inner periphery of SLD, generally coinciding with regions of elevated $\varepsilon(z, x)$. The median value of Ri, $med\,(Ri_{east}) = 1.87$, in stratified waters influenced by SLD dynamics (eastern section, $x > 0$) is lower than the corresponding estimate, $med\,(Ri_{west}) = 3.13$, for the western section $x < 0$.
3. The probability distribution of ε in the interior layer below the density interface ($z > 40$ m) could be well approximated by the Burr distribution, consistent with the proposal by Lozovatsky et al. (2017) for stratified intermittent ocean turbulence.
4. Mixing in SLD pycnocline was quantified in terms of an eddy diffusivity K_N, which is parameterized in terms of the gradient Richardson numberRi. Damping of diapycnal mixing by stratification specified by the power s in equation (2) was found to be relatively strong, with $s = 2$. This value is consistent with the findings of Lozovatsky and Fernando (2013) for mixing in nocturnal stably stratified boundary layers and the well accepted asymptotic formula $K_M \sim \varepsilon/N^2$ for $Ri/Ri_{cr} >> 1$. The damping power $s = 2$ in formula (2) may well be a universal parameter for shear induced turbulence in stratified natural flows, butK_0in (2) is expected to vary with external forcing (external turbulent scales) and background mean shear and stratification. For data obtained at the periphery of SLD, $K_o \approx 1.2 \times 10^{-4}$ m^{2}s^{-1}. Further microstructure measurements are required to better understand relationship between mixing and mesoscale (e.g., SLD) dynamics in the Bay of Bengal, and our study is the first step toward future work.

Acknowledgements

We are grateful to the crew of R/V Thomas G. Thompson, and a group of NARA scientists and technicians for assistance with the VMP measurements. Support for ship operation was provided by the US Office of Naval Research (ONR) and Naval Research Laboratory. We acknowledge funding the participants of University of Notre Dame through ONR grant N00014-17-1-2334. The data, which are shown in Figs. 1–8, are accessible via https://notredame.box.com/s/d8c8npq40st2t01u7yh037u6eragtyxx.

Appendix A. Supplementary data

Supplementary data to this article can be found online at https://doi.org/10.1016/j.dsr2.2019.07.002.

References

Akhil, V.P., Durand, F., Lengaigne, M., Vialard, J., Keerthi, M.G., Gopalakrishna, V.V., Deltel, Papa, C.F., de Boyer Montégut, C., 2014. A modeling study of the processes of surface salinity seasonal cycle in the Bay of Bengal. J. Geophys. Res. Oceans. 119 (6), 3926–3947.

Bhat, G.S., Vecchi, G.A., Gadgil, S., 2004. Sea surface temperature of the Bay of Bengal derived from the TRMM microwave imager. J. Atmos. Ocean. Technol. 21, 1283–1290.

Cummins, P.F., Holloway, G., Gargett, E., 1990. Sensitivity of the GFDL ocean general circulation model to a parameterization of vertical diffusion. J. Phys. Oceanogr. 20 (6), 817–830.

Das, U., Vinayachandran, P.N., Behara, A., 2016. Formation of the southern Bay of Bengal cold pool. Clim. Dyn. 47, 2009–2023. https://doi.org/10.1007/s00382-015-2947-9.

de Vos, A., Pattiaratchi, C.B., Wijeratne, E.M.S., 2014. Surface circulation and upwelling patterns around Sri Lanka. Biogeosciences 11, 5909–5930. https://doi.org/10.5194/bg-11-5909-2014.

Girishkumar, M.S., Ravichandran, M., McPhaden, M.J., Rao, R.R., 2011. Intraseasonal variability in barrier layer thickness in the south central Bay of Bengal. J. Geophys. Res. Oceans. 116, C03009. https://doi.org/10.1029/2010JC006657.

Girishkumar, M.S., Joseph, J., Thangaprakash, V.P., Pottapinjara, V., McPhaden, M.J., 2017. Mixed layer temperature budget for the northward propagating summer monsoon intraseasonal oscillation (MISO) in the central Bay of bengal. J. Geophys. Res. Oceans 122 (11), 8841–8854.

Jinadasa, S.U.P., Lozovatsky, I., Planella-Morató, J., Nash, J.D., MacKinnon, J.A., Lucas, A.J., Wijesekera, H.W., Fernando, H.J.S., 2016. Ocean turbulence and mixing around Sri Lanka and in adjacent waters of the northern Bay of Bengal. Oceanography 29 (2), 170–179. https://doi.org/10.5670/oceanog.2016.49.

Jensen, T.G., Shulman, I., Wijesekera, H., Anderson, S., Ladner, S., 2018. Submesoscale features and their interaction with fronts and internal tides in a high-resolution coupled atmosphere-ocean-wave model of the Bay of Bengal. Ocean Dynam. 68, 391–410. https://doi.org/10.1007/s10236-018-1136-x.

Lozovatsky, I., Roget, E., Figueroa, M., Fernando, H.J.S., Shapovalov, S., 2005. Observations and scaling of the upper mixed layer in the North Atlantic. J. Geophys. Res. Oceans 110, C05013. https://doi.org/10.1029/2004JC002708.

Lozovatsky, I., Roget, E., Figueroa, M., Fernando, H.J.S., Shapovalov, S., 2006. Sheared turbulence in weakly stratified upper ocean. Deep Sea Res. I 53, 387–407.

Lozovatsky, I., Fernando, H.J.S., 2013. Mixing efficiency in natural flows. Phil. Trans. Royal Soc. A 371, 20120213. https://doi.org/10.1098/rsta.2012.0213. 1982.

Lozovatsky, I., Wijesekera, H., Jarosz, E., Lilover, M.-J., Pirro, A., Silver, Z., Centurioni, L., Fernando, H.J.S., 2016. A snapshot of internal waves and hydrodynamic instabilities in the southern Bay of Bengal. J. Geophys. Res. Oceans 121, 5898–5915. https://doi.org/10.1002/2016JC011697.

Lozovatsky, I., Fernando, H.J.S., Planella-Morato, J., Liu, Z., Lee, J.-H., Jinadasa, S.U.P., 2017. Probability distribution of turbulent kinetic energy dissipation rate in ocean: observations and Approximations. J. Geophys. Res. Oceans 122, 8293–8308. https://doi.org/10.1002/2017JC013076.

Munk, W.H., Anderson, E.R., 1948. Notes on the theory of the thermocline. J. Mar. Res. 3, 276–295.

Pacanowski, R.C., Philander, S.G.H., 1981. Parameterization of vertical mixing in numerical models of tropical oceans. J. Phys. Oceanogr. 11, 1443–1451.

Padman, L., Dillon, T.M., 1991. Turbulent mixing near the yermak plateau during the coordinate eastern arctic experiment. J. Geophys. Res. 96, 4769–4782.

Paka, V.T., Nabatov, V.N., Lozovatsky, I.D., Dillon, T.M., 1999. Ocean microstructure measurements by BAKLAN and GRIF. J. Atmos. Ocean. Technol. 16, 1519–1532.

Parampil, S.R., Gera, A., Ravichandran, M., Sengupta, D., 2010. Intraseasonal response of mixed layer temperature and salinity in the Bay of Bengal to heat and freshwater flux. J. Geophys. Res. 115, C05002. https://doi.org/10.1029/2009JC005790.

Pelegri, J.L., Csanady, G.T., 1994. Dyapicnal mixing in western boundary currents. J. Geophys. Res. 99, 18275–18304.

Peters, H., Gregg, M.C., Tool, J.M., 1988. On the parameterization of equatorial turbulence. J. Geophys. Res. 93, 1199–1218.

Pollard, R.T., Rhines, P.B., Thompson, R., 1972. The deepening of the wind-mixed layer. Geophys. Fluid Dyn. 4 (1), 381–404.

Roget, E., Lozovatsky, I., Sanchez, X., Figueroa, M., 2006. Microstructure measurements in natural waters: methodology and applications. Prog. Oceanogr. 70, 123–148.

Shetye, S.R., 1993. The movement and implications of the Ganges-Brahmaputra runoff on entering the Bay of Bengal. Curr. Sci. 64 (1), 32–38 ISSN 0011–3891.

Shetye, S.R., Gouveia, A.D., Shankar, D., Shenot, S.S.C., Vinayachandran, P.N., Sundar, D., Michael, G.S., Nampoothiri, G., 1996. Hydrography and circulation in the western Bay of Bengal during the northeast monsoon. J. Geophys. Res. Oceans 101, 14011–14025.

Shroyer, E.L., Rudnick, D.L., Farrar, J.T., Lim, B., Venayagamoorthy, S.K., St Laurent, L.C., Garanaik, A., Moum, J.N., 2016. Modification of upper-ocean temperature structure by subsurface mixing in the presence of strong salinity stratification. Oceanography 29 (2), 62–71. https://doi.org/10.5670/oceanog.2016.39.

Soloviev, A., Lukas, R., Hacker, P., 2001. An approach to parameterization of the oceanic turbulent boundary layer in the western Pacific warm pool. J. Geophys. Res. 106, 4421–4435.

Vinayachandran, P.N., Yamagata, T., 1998. Monsoon response of the sea around Sri Lanka: generation of thermal domes and anticyclonic vortices. J. Phys. Oceanogr. 28, 1946–1960.

Wijesekera, H.W., Jensen, T.G., Jarosz, E., Teague, W.J., Metzger, E.J., Wang, D.W., Jinadasa, U., Arulananthan, K., Centurioni, L., Fernando, H.J.S., 2015. Southern Bay of Bengal currents and salinity intrusions during a fall monsoon transition. J. Geophys. Res. Oceans 120 (10), 6897–6913. https://doi.org/10.1002/2015JC010744.

Wijesekera, H.W., et al., 2016,aa. ASIRI: an ocean-atmosphere initiatives for Bay Bengal. Bull. Amer. Met. Soc. 1859–1884. https://doi.org/10.1175/BAMS-D-14-00197.1.

Wijesekera, H.W., Teague, W.J., Wang, D.W., Jarosz, E., Jensen, T.G., Jinadasa, S.U.P., Fernando, H.J.S., Hallock, Z.R., 2016,bb. Low-frequency currents from deep moorings in the southern Bay of bengal. J. Phys. Oceanogr. 46, 3209–3238. https://doi.org/10.1175/JPO-D-16-0113.1.